ChemComm

Tuning the Pore Chemistry of Zr-MOFs for Efficient Metal Ion Capture from Complex Streams

Journal:	*ChemComm*
Manuscript ID	CC-COM-01-2024-000320.R1
Article Type:	Communication

COMMUNICATION

Tuning the Pore Chemistry of Zr-MOFs for Efficient Metal Ion Capture from Complex Streams

Received 00th January 20xx,
Accepted 00th January 20xx

DOI: 10.1039/x0xx00000x

R. Eric Sikma,[a] Boyoung Song,[b] Jacob I. Deneff,[a] Jacob Smith,[b] Kadie Sanchez,[b] Raphael A. Reyes,[a] Luke M. Lucero,[a] Keith J. Fritzsching,[c] Anastasia G. Ilgen,[b] Dorina F. Sava Gallis*[a]

Metal-organic frameworks (MOFs) have shown promise for adsorptive separations of metal ions. Herein, MOFs based on highly stable Zr(IV) building units were systematically functionalized with targeted metal binding groups. Through competitive adsorption studies, it was shown that the selectivity for different metal ions was directly tunable through functional group chemistry.

The continued growth and diversification of technology and the energy landscape have resulted in increasing demand for transition metals and rare-earth elements (REEs).[1, 2] Transition metals, such as Mn, Co, and Ni, are important elements in modern batteries, which are critical for the development of renewable energy.[3] REEs have found widespread use in electronics, batteries, magnetic materials, catalysis, wind energy, and other areas.[1, 4] The global supply of many transition metals and REEs is limited, hence many of them are defined as "critical elements," and the geopolitical landscape can create supply chain issues.[1, 5] Concurrently, ever-increasing amounts of waste materials that contain these valuable metals are being generated. Recovery and recycling of metals from these waste streams is essential in order to realize a sustainable, circular economy.[5] However, the ions of interest may only be present in low concentrations and are often distributed in complex aqueous matrices, creating a significant purification challenge.[6]

Adsorptive separation of metal ions presents a possible solution to these drawbacks.[7] In this case, a selective porous material is used to adsorb specific ions from mixed-ion solutions.[8] The material can then be removed and the adsorbed ions can be recovered by mild acidic leaching.[9] This represents an energy-efficient process that generates minimal waste and offers the ability to capture ions that are present in low concentrations (e.g., from waste streams). Furthermore, with reversible adsorption these materials can be continuously re-used. For this process to be viable, materials with high adsorption capacity and selectivity for the ion(s) of interest are needed. However, engineering these properties into porous materials is a significant challenge.

Metal-organic frameworks (MOFs) are crystalline materials constructed by the connection of metal ions or clusters through organic linkers with two or more metal binding groups.[10] These materials display exceptional porosity and a degree of tunability that is unrivalled in materials chemistry. MOFs have shown promise for numerous applications, including aqueous ion separations.[9, 11, 12] Their atomically precise structures enable controllable design of targeted metal binding sites.[13] Zr(IV) MOFs in particular have excellent stability to aqueous and acidic conditions and are thus well suited for metal ion separations.[14]

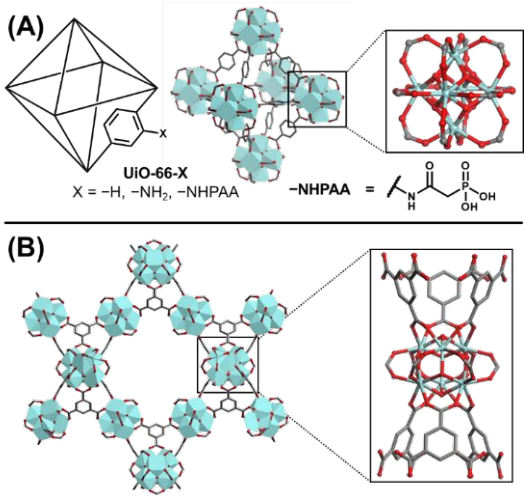

Fig. 1 Representations of pore cavities and Zr_6 building units of (A) UiO-66 and (B) MOF-808 from crystal structure data; (A) highlights functional groups installed in UiO-66 in this work; C = gray, O = red, Zr = teal; H atoms omitted for clarity.

Two distinct Zr-MOF families were chosen to probe the influence of defect character and functional groups on selective

[a] *Nanoscale Sciences Department, Sandia National Laboratories, Albuquerque, NM 87185, United States. Email: dfsava@sandia.gov*
[b] Geochemistry Department, Sandia National Laboratories, Albuquerque, NM 87185, United States
[c] *Organic Materials Science Department, Sandia National Laboratories, Albuquerque, NM 87185, United States*

†Electronic Supplementary Information (ESI) available: Synthetic methods and additional characterization data. See DOI: 10.1039/x0xx00000x

metal ion capture from complex streams: (1) UiO-66 was selected as a smaller pore (ca. 8-11 Å) platform due the wide array of possible organic linker functionalizations and the ability to predictably control defect character;[15] (2) MOF-808 was chosen due to its distinct topology, larger pore size (up to 18 Å), and the ability to install a broad range of functionalities by coordination to the Zr(IV) clusters (*vide infra*).[16]

First, the roles of defects and linker functional groups were investigated. A series of UiO-66-based materials was targeted with variable defect character and linker functionalities (Figure 1A). With UiO-66 as the parent material, amino-functionalized UiO-66-NH_2 was chosen due to the basicity of the $-NH_2$ groups, which could serve as metal binding sites and/or alter the pH of the pore environment. UiO-66 and UiO-66-NH_2 were synthesized in both low-defect (LD) and high-defect (HD) forms following literature procedures, specifically targeting missing-linker defects, giving a total of four materials.[17-19] In place of the missing linkers, the Zr clusters contain terminal hydroxide, water, chloride, and/or formate ligands, which could serve as metal binding sites. Thermogravimetric analysis (TGA) confirmed the variable defect character in these samples (Figures S1-S2). Bulk crystallinity and phase purity of the MOFs were confirmed by powder X-ray diffraction (PXRD) (Figure 2, left), and N_2 physisorption analysis at 77 K demonstrated permanent porosity for each material (Figure 2, right). The internal surface areas of the MOFs were calculated from the N_2 isotherms by the Brunauer-Emmett-Teller (BET) method, which gave values of 1390 (UiO-66(LD)), 1920 (UiO-66(HD)), 850 (UiO-66-NH_2(LD)), and 1190 (UiO-66-NH_2(HD)) $m^2\ g^{-1}$. The significantly larger surface areas on the HD materials further confirmed their higher degrees of defects.

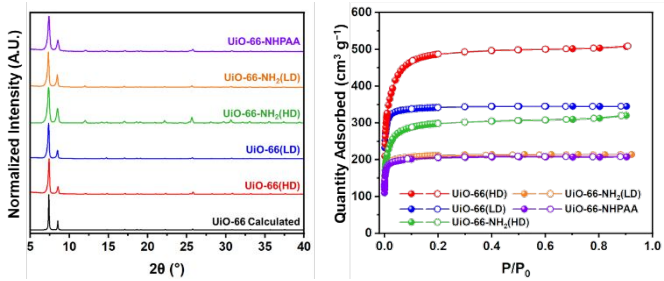

Fig. 2 PXRD patterns (left) and N_2 sorption isotherms (right) collected at 77 K of UiO-66(HD) (red), UiO-66(LD) (blue), UiO-66-NH_2(HD) (green), UiO-66-NH_2(LD) (orange), and UiO-66-NHPAA (purple); calculated PXRD pattern of UiO-66 shown in black.

Subsequently, due to the expected high affinity of phosphonate groups for REEs, a method was developed to install a phosphonate functionality in UiO-66.[20] Based on known post-synthetic modification (PSM) chemistry, phosphonoacetic acid (PAA) was appended to UiO-66-NH_2(LD) through amide linkages to generate UiO-66-NHPAA (Figure 3A).[21] The LD version of UiO-66-NH_2 was used to minimize binding of PAA directly to the Zr(IV) clusters at defect sites. The conversion was achieved by refluxing a suspension of the MOF in an acetonitrile solution containing PAA, with (N,N'-dicyclohexylcarbodiimide) (DCC) used as a dehydrating agent. The PSM reaction proceeded with retention of crystallinity, as confirmed by PXRD (Figure 2), and infrared (IR) spectroscopy confirmed the successful generation of amide linkages and the incorporation of phosphonate groups (Figure S3). UiO-66-NHPAA maintained a high degree of porosity, with a BET surface area of 810 $m^2\ g^{-1}$ (Figure 2, right).

UiO-66-NHPAA was further studied by solid-state cross-polarization (CP) magic-angle spinning (MAS) ^{13}C and ^{31}P nuclear magnetic resonance spectroscopy (NMR). Fitting the ^{13}C spectrum of UiO-66-NHPAA (Figure 3C) and comparison to the ^{13}C spectrum of UiO-66-NH_2(LD) (Figure 3B) revealed that ca. 60% of the UiO-66-NH_2 amino groups were converted to −NHPAA. Interestingly, the ^{31}P spectrum revealed a total of 3 phosphorus environments (Figure S4). The major peak was ascribed to the −NHPAA groups, while the two smaller peaks were assigned as PAA bound directly to defect sites on the Zr clusters through either the phosphonate or the acetate groups.

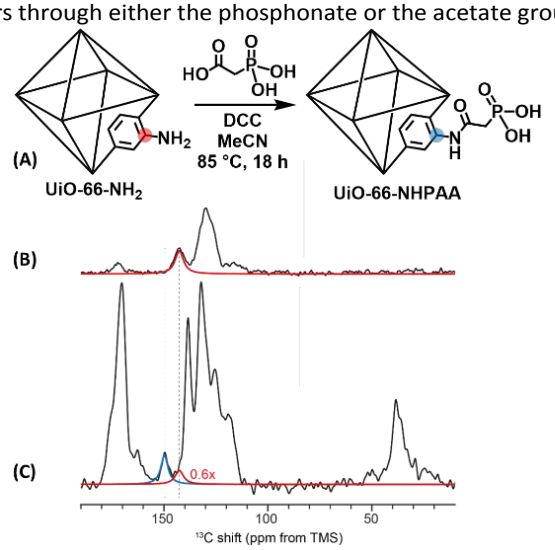

Fig. 3 (A) Synthetic scheme for conversion of UiO-66-NH_2 into UiO-66-NHPAA, highlighting C atoms used for NMR quantification (red and blue); ^{13}C [^1H] CP MAS NMR spectra of (B) UiO-66-NH_2(LD) and (C) UiO-66-NHPAA.

Next, a series of MOF-808 derivatives was synthesized to investigate the effects of cluster-based functional groups. The hexanuclear Zr(IV) building units of MOF-808 are 6-connected through 1,3,5-benzenetricarboxylate (BTC) linkers and are capped by 6 terminal μ_2-bridging formate ligands (Figure 1B).[16] These formate groups can be readily exchanged for a range of functionalized carboxylates by post-synthetic treatment of the MOF with an excess of the corresponding carboxylic acids.[11, 12] MOF-808 was synthesized according to a modified literature protocol, then treated with 4 different carboxylic acids bearing additional metal-binding groups: pyrazole-4-carboxylic acid (PyC), diethylphosphonoacetic acid (Et_2PAA), aspartic acid (AA), and sodium 3-sulfoisophthalic acid (BDC-SO_3) (Scheme 1).[12, 22] These were installed by heating suspensions of pristine MOF-808 in aqueous or DMF solutions of the desired carboxylic acids (5 eq. per Zr, or 2.5 eq. per Zr for Et_2PAA).

Functional groups with varying basicity and donor strength were used to evaluate the effectiveness of different ligand types, including pyrazolyl, diethylphosphono, carboxylic acid, amino, and sulfonate. These were targeted due to their differing acid-base properties and expected binding affinities. Because phosphonate groups would preferentially coordinate to the Zr clusters, an ethyl-protected version of PAA was used to ensure

binding through the carboxylate. The 4 corresponding mono-functionalized MOF-808 derivatives (MOF-808-PyC, MOF-808-Et_2PAA, MOF-808-AA, and MOF-808-BDC-SO_3) were generated, and a bifunctional material (MOF-808-AA/BDC-SO_3) was also synthesized in order to assess potential cooperative binding effects. This was achieved in one step by treating MOF-808 with an equimolar solution of AA and BDC-SO_3 in water. It should be noted that this one-pot approach to achieve multifunctional MOF-808 derivatives may prove to be broadly useful for fine-tuning the properties of MOF-808 for a variety of applications.

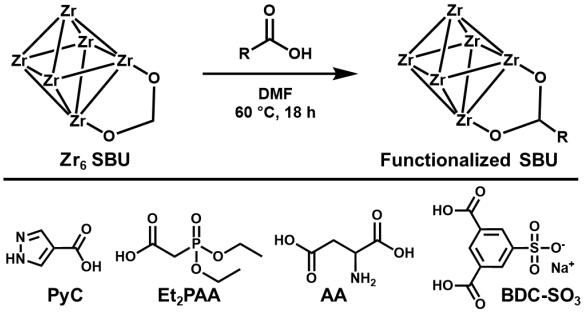

Scheme 1 Post-synthetic exchange of formate groups on MOF-808 Zr_6 clusters (top) and structures of functionalized carboxylic acids installed in MOF-808 in this work (bottom).

Each MOF-808 derivative retained crystallinity after PSM, as demonstrated by PXRD (Figure 4, left), and successful incorporation of the desired functional groups was confirmed by infrared (IR) spectroscopy (Figures S5-S9). The materials displayed decreased N_2 uptake compared to unfunctionalized MOF-808 (Figure 4), which was expected due the occupancy of pore space by the added functional groups. However, each MOF remained highly porous after functionalization, with BET surface areas of 1460 (MOF-808-PyC), 1200 (MOF-808-Et_2PAA), 1360 (MOF-808-AA), 1180 (MOF-808-BDC-SO_3), and 1270 (MOF-808-AA/BDC-SO_3) $m^2\ g^{-1}$, compared to 1680 $m^2\ g^{-1}$ for unmodified MOF-808.

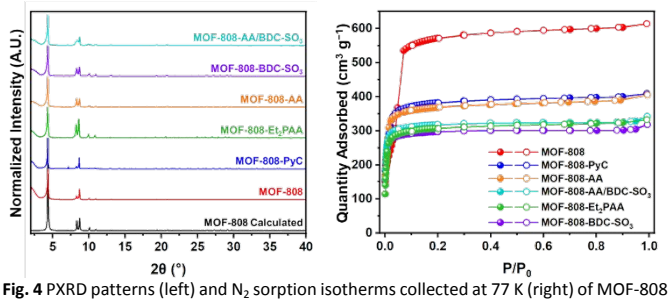

Fig. 4 PXRD patterns (left) and N_2 sorption isotherms collected at 77 K (right) of MOF-808 (red), MOF-808-PyC (blue), MOF-808-Et_2PAA (green), MOF-808-AA (orange), MOF-808-BDC-SO_3 (purple), and MOF-808-AA/BDC-SO_3 (teal); calculated PXRD pattern of MOF-808 shown in black.

The MOF-808 derivatives were digested in KOD/D_2O and analysed by ^{1}H NMR to quantify the degrees of functionalization (Figures S10-S22). It was found that at least two functional groups per Zr cluster were incorporated in each material (Table S1). Intuitively, the smaller functional groups generally gave higher degrees of incorporation. MOF-808-AA/BDC-SO_3 was found to contain nearly equimolar quantities of both functional groups, closely matching the ratio in the PSM reaction solution.

The performance of the UiO-66 and MOF-808 derivatives series was assessed through competitive, multi-component ion adsorption experiments at semi-neutral pH. A low concentration (0.20 mM) of each ion was used to simulate recovery from dilute waste streams, with four total ions in solution: Nd^{3+}, Lu^{3+}, Co^{2+}, and Ni^{2+}. Nd and Lu were chosen as representative REE ions with different ionic radii (Nd^{3+} = 0.98 Å, Lu^{3+} = 0.86 Å).[23] Co^{2+} (r = 0.75 Å) and Ni^{2+} (r = 0.69 Å) were chosen as competitive transition metal ions, as separation of Co and Ni from waste streams is important for battery recycling.[3] Activated MOF powders were immersed in the mixed-ion solution (buffered to a pH of 6.5) for 24 h. A long exposure time was chosen so that the results would primarily reflect the thermodynamics of adsorption, mitigating the kinetic effects of differing pore sizes. The concentrations of the ions in solution were determined by inductively coupled plasma-mass spectrometry (ICP-MS) before and after treatment with the MOFs, with the difference corresponding to the amounts adsorbed by the materials. The results of these experiments are presented in Figure 5 as removal percentages.

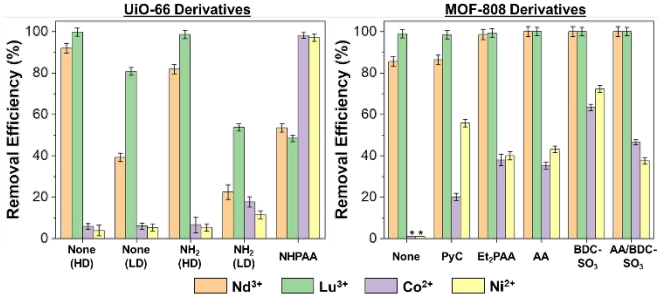

Fig. 5 Bar graphs showing results of competitive ion adsorption studies as removal percentages (removal efficiencies) for the different ions (from left to right: Nd^{3+} = orange, Lu^{3+} = green, Co^{2+} = purple, and Ni^{2+} = yellow) for each material. UiO-66 data is shown on the left, with legend indicating linker-based functional groups and defectiveness. MOF-808 data is shown on the right, with legend indicating functional groups appended to the Zr clusters. *MOF-808 displayed no measurable uptake of Co^{2+} or Ni^{2+}.

Interestingly, UiO-66 and UiO-66-NH_2 gave excellent selectivity for the 3+ REEs over the 2+ transition metals. Defect character was found to drastically impact the performance of these materials. The more defective versions (UiO-66(HD) and UiO-66-NH_2(HD)) gave high removal percentages for both Nd and Lu, indicating that defect sites may be important binding sites for REE ions.[24] The low-defect materials (UiO-66(LD) and UiO-66-NH_2(LD)) gave lower REE removal efficiencies but greatly enhanced selectivity for Lu over Nd, suggesting a trade-off between removal efficiency and selectivity. Presumably, the lower numbers of defect sites in the LD materials correspond to fewer strong binding sites for REE ions, resulting in increased competition for binding sites and enhanced selectivity.

Surprisingly, UiO-66-NHPAA was found to have significant selectivity for the 2+ transition metals over the 3+ REEs, despite the anticipated high affinity of phosphonate groups for REE ions. The Co and Ni removal efficiencies were greatly increased in UiO-66-NHPAA relative to the parent material (UiO-66-NH_2(LD)), indicating strong interactions between the PAA groups and these ions. Indeed, the Co and Ni removal percentages of UiO-66-NHPAA (98% and 97%, respectively)

were the highest for the series of materials tested in this work by a large margin. The selectivity for the smaller ions (Ni^{2+} and Co^{2+}, r = 0.75 and 0.69 Å, respectively) may be a result of the bulky PAA groups occupying pore volume.

Despite the significant topological differences, unfunctionalized MOF-808 performed similarly to UiO-66(HD), removing 3+ REE ions with high efficiency while displaying negligible uptake of the 2+ metals. The slight preference for Lu^{3+} over Nd^{3+} was also consistent with the UiO series. These similarities point to the Zr clusters as important binding sites for REE ions, as the Zr_6 building unit is the primary commonality between MOF-808 and UiO-66. The marked selectivity of both Zr-MOF platforms for 3+ REEs indicates that these cluster sites are inherently selective for the harder 3+ ions. Appending competent metal binding groups (i.e., PyC, Et_2PAA, AA, BDC-SO_3) was found to generally increase the uptake of the transition metal ions with diminished selectivity for REEs.

Significantly, MOF-808-PyC gave nearly 3:1 selectivity for Ni^{2+} over Co^{2+}, which are typically difficult to separate at semi-neutral conditions. This indicates that the pyrazolyl groups have higher affinity for Ni over Co, likely due to their ability to act as a π-acceptor ligands, inferring that MOF-808-PyC could be a viable material for the adsorptive separation of Ni and Co. The Co^{2+} and Ni^{2+} removal efficiencies of MOF-808-BDC-SO_3 were the highest in the MOF-808 series, likely due to the presence of two available binding groups per appended molecule (−COOH and $-SO_3^-$). The MOF-808 series generally showed a slight preference for Ni^{2+} over Co^{2+}, with the exception of MOF-808-AA/BDC-SO_3. This MOF displayed different Co/Ni selectivity than both corresponding monofunctional materials, with a modestly higher affinity for Co. This was an unexpected result, which suggests that the AA and BDC-SO_3 groups function cooperatively in the bifunctional material.

Importantly, all materials were found to retain crystallinity after the competitive adsorption experiments by PXRD (Figures S23-S24). Zr(IV) MOFs may therefore prove to broadly useful for aqueous metal ion separations. In conclusion, control of defect character and functional groups in Zr(IV) MOFs was shown to define their capacities and selectivities for transition metal and REE ions. This approach can be utilized to design ion-selective capture materials, which will have significant industrial relevance in developing energy-efficient separations.

This work was supported by the Laboratory Directed Research and Development Program at Sandia National Laboratories. This article has been authored by an employee of National Technology & Engineering Solutions of Sandia, LLC under Contract No. DE-NA0003525 with the U.S. Department of Energy (DOE). The employee owns all right, title and interest in and to the article and is solely responsible for its contents. The United States Government retains and the publisher, by accepting the article for publication, acknowledges that the United States Government retains a non-exclusive, paid-up, irrevocable, world-wide license to publish or reproduce the published form of this article or allow others to do so, for United States Government purposes. The DOE will provide public access to these results of federally sponsored research in accordance with the DOE Public Access Plan https://www.energy.gov/downloads/doe-public-access-plan.

Conflicts of interest

There are no conflicts to declare.

Notes and references

1 E. Alonso, A. M. Sherman, T. J. Wallington, M. P. Everson, F. R. Field, R. Roth and R. E. Kirchain, *Environ. Sci. Technol.*, 2012, **46**, 3406-3414.
2 W. Lee, J. Kim, S. Yun, W. Choi, H. Kim and W.-S. Yoon, *Energy Environ. Sci.*, 2020, **13**, 4406-4449.
3 L. Yang, G. Xi and Y. Xi, *Ceram. Int.*, 2015, **41**, 11498-11503.
4 K. M. Goodenough, F. Wall and D. Merriman, *Nat. Resour. Res.*, 2018, **27**, 201-216.
5 N. Swain and S. Mishra, *J. Clean. Prod.*, 2019, **220**, 884-898.
6 B. Kronholm, C. G. Anderson and P. R. Taylor, *JOM*, 2013, **65**, 1321-1326.
7 X. Sun, H. Luo, S. M. Mahurin, R. Liu, X. Hou and S. Dai, *J. Rare Earths*, 2016, **34**, 77-82.
8 M. Traore, A. Gong, Y. Wang, L. Qiu, Y. Bai, W. Zhao, Y. Liu, Y. Chen, Y. Liu, H. Wu, S. Li and Y. You, *J. Rare Earths*, 2023, **41**, 182-189.
9 I. Ahmed, Y.-R. Lee, K. Yu, S. Bhattacharjee and W.-S. Ahn, *Ind. Eng. Chem. Res.*, 2019, **58**, 2324-2332.
10 H. Furukawa, K. E. Cordova, M. O'Keeffe and O. M. Yaghi, *Science*, 2013, **341**, 1230444.
11 Y. Peng, H. Huang, Y. Zhang, C. Kang, S. Chen, L. Song, D. Liu and C. Zhong, *Nat. Commun.*, 2018, **9**, 187.
12 A. Valverde, G. I. Tovar, N. A. Rio-López, D. Torres, M. Rosales, S. Wuttke, A. Fidalgo-Marijuan, J. M. Porro, M. Jiménez-Ruiz, V. García Sakai, A. García, J. M. Laza, J. L. Vilas-Vilela, L. Lezama, M. I. Arriortua, G. J. Copello and R. Fernández de Luis, *Chemistry of Materials*, 2022, **34**, 9666-9684.
13 M. Carboni, C. W. Abney, S. Liu and W. Lin, *Chem. Sci.*, 2013, **4**, 2396-2402.
14 S. Yuan, J.-S. Qin, C. T. Lollar and H.-C. Zhou, *ACS Cent. Sci.*, 2018, **4**, 440-450.
15 J. H. Cavka, S. Jakobsen, U. Olsbye, N. Guillou, C. Lamberti, S. Bordiga and K. P. Lillerud, *J. Am. Chem. Soc.*, 2008, **130**, 13850-13851.
16 H. Furukawa, F. Gándara, Y.-B. Zhang, J. Jiang, W. L. Queen, M. R. Hudson and O. M. Yaghi, *J. Am. Chem. Soc.*, 2014, **136**, 4369-4381.
17 G. C. Shearer, S. Chavan, J. Ethiraj, J. G. Vitillo, S. Svelle, U. Olsbye, C. Lamberti, S. Bordiga and K. P. Lillerud, *Chemistry of Materials*, 2014, **26**, 4068-4071.
18 L. Yuan, M. Tian, J. Lan, X. Cao, X. Wang, Z. Chai, J. K. Gibson and W. Shi, *Chem. Commun.*, 2018, **54**, 370-373.
19 G. W. Peterson, M. R. Destefano, S. J. Garibay, A. Ploskonka, M. McEntee, M. Hall, C. J. Karwacki, J. T. Hupp and O. K. Farha, *Chem. Eur. J.*, 2017, **23**, 15913-15916.
20 F. Xie, T. A. Zhang, D. Dreisinger and F. Doyle, *Minerals Engineering*, 2014, **56**, 10-28.
21 J. de Decker, J. de Clercq, P. Vermeir and P. van der Voort, *J. Mater. Sci.*, 2016, **51**, 5019-5026.
22 J. Jiang, F. Gándara, Y.-B. Zhang, K. Na, O. M. Yaghi and W. G. Klemperer, *J. Am. Chem. Soc.*, 2014, **136**, 12844-12847.
23 R. D. Shannon, *Acta Crystallogr. A*, 1976, **32**, 751-767.
24 X. Ren, C.-C. Wang, Y. Li, P. Wang and S. Gao, *Journal of Hazardous Materials*, 2023, **445**, 130552.